13. Kosovichev A G et al., in *Sounding Solar Stellar Interiors: Proc. of the 181st Symp. of Intern. Astron. Union, Nice, France, September 30 – October 3, 1996* (Eds J Provost, F-X Schmider) (Dordrecht: Kluwer Acad. Publ., 1997) p. 203
14. Spiegel E A, Zahn J-P *Astron. Astrophys.* **265** 106 (1992)
15. Parker E N *Cosmical Magnetic Fields: Their Origin and Their Activity* (Oxford: Clarendon Press, 1979) [Translated into Russian: Vol. 1 (Moscow: Mir, 1982) p. 412]
16. Kuznetsov V D, Syrovatskii S I *Astron. Zh.* **56** 1263 (1979) [*Sov. Astron.* **23** 715 (1979)]
17. Kuznetsov V D *Magnitnaya Gidrodinamika* **2** 13 (1987)
18. Kuznetsov V D, in *Physics of Magnetic Flux Ropes* (Geophys. Monograph, Vol. 58, Eds C T Russell, E R Priest, L C Lee) (Washington, DC: American Geophys. Union, 1990) p. 77
19. Schrijver C J et al. *Astrophys. J.* **628** 501 (2005)
20. Syrovatskii S I, Bulanov S V, Dogel' V A "Fizika solnechnykh vspyshek" ("Physics of solar flares"), in *Itogi Nauki i Tekhniki Ser. Astronomiya* (Progress in Science and Technology. Ser. Astronomy) Vol. 21 (Moscow: VINITI, 1982) p. 188
21. Priest E, Forbes T *Magnetic Reconnection: MHD Theory and Applications* (Cambridge: Cambridge Univ. Press, 2000) [Translated into Russian (Moscow: Fizmatlit, 2005) p. 352]
22. Kuznetsov V D, Syrovatskii S I *Solar Phys.* **69** 361 (1981)
23. Kuznetsov V D *Astron. Zh.* **59** 108 (1982) [*Sov. Astron.* **26** 67 (1982)]
24. *Space News* **16** (33) 16 (2005); *Raketnaya Kosmicheskaya Tekh.* (TsNIIMASh) (41) 2 (2005)
25. Syrovatskii S I *Pis'ma Astron. Zh.* **2** 35 (1976) [*Sov. Astron. Lett.* **2** 13 (1976)]
26. Heyvaerts J, Priest E R, Rust D M *Astrophys. J.* **216** 123 (1977)
27. Schmieder B et al. *Solar Phys.* **150** 199 (1994)
28. Kuznetsov V D *Solnechnye Dannye* (Bull.) (7) 83 (1985)
29. Priest E R, Heyvaerts J F, Title A M *Astrophys. J.* **576** 533 (2002)
30. Gamayunov K V, Oraevsky V N, Kuznetsov V D *Plasma Phys. Control. Fusion* **40** 1285 (1998)
31. Saint-Hilaire P, Benz A O *Solar Phys.* **210** 287 (2002)
32. Kuznetsov V D, in *Itogi Nauki i Tekhniki Ser. Astronomiya* (Progress in Science and Technology. Ser. Astronomy) Vol. 45 (Moscow: Kosmosinform, 1994) p. 3
33. Dere K P, Wang J, Yan Y (Eds) *Coronal and Stellar Mass Ejections: Proc. IAU Symp.* No. 226 (Cambridge: Cambridge Univ. Press, 2005)
34. Leka K D et al. *Astrophys. J.* **462** 547 (1996)
35. Burlaga L F *Planet. Space Sci.* **49** 1619 (2001)
36. Priest E R *Solar Magnetohydrodynamics* (Dordrecht: D. Reidel Publ. Co., 1984) [Translated into Russian (Moscow: Mir, 1985) p. 189]
37. Kuznetsov V D, Hood A W *Solar Phys.* **171** 61 (1997)
38. Kuznetsov V D, Hood A W *Adv. Space Res.* **26** 539 (2000)
39. Burlaga L F et al. *Science* **309** 2027 (2005)
40. Jokipii J R, Giacalone J *Astrophys. J.* **605** L145 (2004)
41. Baranov V B, Fahr H J *J. Geophys. Res.* (*Space Phys.*) **108** (A3) 1110 (2003)
42. Kuznetsov V D, Nakaryakov V M, Tsyganov P V *Pis'ma Astron. Zh.* **21** 793 (1995) [*Astron. Lett.* **21** 710 (1995)]
43. Marsch E et al., in *Proc. of the Conf. Crossroads for European Solar and Heliospheric Space Physics, Puerto de la Cruz, Tenerife, Spain, March 23 – 27, 1998* (ESA SP, No. 417, Eds E R Priest, F Moreno-Insertis, R A Harris) (Noordwijk, The Netherlands: ESA Publ. Division, 1998) p. 91
44. Kuznetsov V D *Zemlya Vselennaya* (2) 18 (2000)

PACS numbers: **96.60.–j**, 96.60.Pb, 97.10.Jb
DOI: 10.1070/PU2006v049n03ABEH005968

Problems of solar activity physics

V V Zaitsev, A V Stepanov

1. Introduction

The energy emitted by the Sun ('the solar luminosity', 3.86×10^{26} W) determines almost all processes on the Earth. Although the solar bolometric luminosity is 3 – 4 orders of magnitude higher than the power of flares and solar ejections of matter, it is these phenomena that have a significant impact on the situation in the circumterrestrial space, ionosphere, and the terrestrial atmosphere. Solar flares are accompanied by plasma heating, charged particle acceleration, eruptive phenomena and electromagnetic energy generation in a wide wavelength range from the gamma-rays to radio band, and most completely reflect the concept of a solar activity.

In 2007, under the auspices of the United Nations Organization, the scientific program International Heliophysical Year (IHY) will begin. This program, like the program International Geophysical Year executed 50 years ago, should join efforts of solar researchers and geophysicists from around the world to formulate and solve important problems concerning the origin of solar activity, the prognosis of active solar phenomena, and their impact on the Earth.

In this report we discuss actual problems of the physics of solar flares, which include mechanisms of flaring energy release; mechanisms of charged particle acceleration and features of their propagation, and the problem of flaring plasma diagnostics. Prospects for solving these problems are illustrated by the example of coronal magnetic arches — fundamental structures in the solar atmosphere and in flare stars.

2. The origin of a flare. Equivalent electric circuit

Most likely, there is no universal mechanism for describing different features of solar flares (C de Jager: "*Flares are different*"). More than ten models and their modifications are being discussed in the current literature. A developed solar flare possesses a complex magnetic configuration consisting of a set of arches (loops) with a characteristic size of $10^9 - 10^{10}$ cm. Such a structure is also observed in late-type stars. The most popular current models comprise the model of interacting magnetic loops [1, 2]; flares in the coronal streamer [3]; the model with outgoing magnetic flux [4]; 'statistical' flares [5], and models of single flare loops [6, 7]. These models, as a rule, invoke the mechanism of 'reconnection' of magnetic field lines, studied by Syrovatskii [8] and Somov [9].

The 'electric circuit' model proposed by Alfvén and Carlqvist [10] is based on measurements made by Severnyi (see Ref. [11]), who discovered electric currents $I \geqslant 10^{11}$ A in the vicinity of solar spots, and on the analogy to a circuit with mercury rectifier capable of producing a sharp transition from a high-conductivity state to that with a great resistance. At the instant of breaking the current in the circuit, an explosive energy release occurs. It is crucial to understand the mechanisms of the current 'breaking'. By developing the model [10], we accounted for the following: (1) a flare is principally a nonstationary process, so that the stationary Ohm law $\mathbf{j} = \sigma \mathbf{E}$ is inapplicable for describing the flare, and (2) the neutral plasma component plays a decisive role in the electric current energy dissipation.

2.1 The model of a single loop flare with current

Data from optical, X-ray (SMM, Yohkoh, TRACE, RHESSI, CORONAS-F) and radio observations (VLA, NoRH, SSRT) indicate that quite frequently solar flares are registered as occurring in isolated arches (single loop flares)

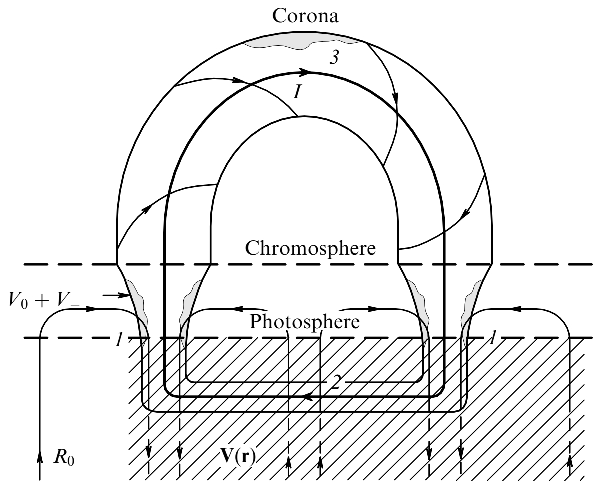

Figure 1. Schematic of a coronal magnetic loop formed by the convergent convective fluxes of photospheric plasma. $\mathbf{V}(\mathbf{r})$ is the matter velocity.

located far away from solar spots [7, 11]. Let us consider electrodynamical processes occurring in single flare loops, which is important both for the interpretation of single arches and for the understanding of the physics of flares with a complex magnetic structure.

Simple estimates [12, 13] show that the electric current energy stored in an arch, $W = LI^2/2$, with a magnetic arch's inductivity $L \sim 10$ H and current $I \sim 10^{11} - 10^{12}$ A amounts to $5 \times 10^{22} - 5 \times 10^{24}$ J, which is sufficient for a solar flare. However, the power released at classical (Spitzer) resistance of the arch $R \sim 10^{-11}\ \Omega$ is around $\mathrm{d}W/\mathrm{d}t = RI^2 \sim 10^{11} - 10^{13}$ W, which is 8 – 10 orders of magnitude smaller than that of a solar flare. The flare will occur if the resistance increases up to $10^{-4} - 10^{-2}\ \Omega$, which is equivalent to current breaking. The reason for the significant increase in the circuit resistance is one of the main problems in the theory of flares. The 'electric circuit' model was further developed in Refs [12 – 18].

Figure 1 displays a magnetic loop rooted in the photosphere, whose footpoints are formed by converging fluxes of photospheric matter. Such a situation occurs when the footpoints of the loop are located at the nodes of several supergranulation cells. The existence of strong electric currents in coronal arches is confirmed by observations [19] and the TRACE data that suggest a virtually constant cross section of the arch along its length, which is unlikely for a potential magnetic field. In this structure, three regions can be separated.

In region 1 located in the photosphere, a magnetic field with associated consistent electric current is generated. In this region, $\omega_e/\nu_{ea} \gg 1$, $\omega_i/\nu_{ia} \ll 1$, where ω_e and ω_i are gyrofrequencies of electrons and ions, respectively, and ν_{ea} and ν_{ia} are the electron – atom and the ion – atom collision frequencies, respectively. Electrons, then, are magnetized and ions are dragged by the neutral plasma component, which gives rise to a radial electric charge-separating field E_r [14]. The field E_r along with the original magnetic field B_z generate the Hall current j_φ that strengthens B_z [20]. The magnetic field is strengthened until the 'raking' of the background magnetic field is compensated by the magnetic field diffusion due to anisotropic plasma conductivity. As a result, a stationary magnetic flux tube is formed in which the magnetic field is determined by the total energy deposition of the convective plasma flux over the tube formation time (around R_0/V_r, where $R_0 \sim 30{,}000$ km is the supergranulation cell scale, and $V_r \sim 0.1 - 0.5$ km s^{-1} is the horizontal velocity of the convective motion). The magnetic field energy density inside the tube can strongly exceed the density of the kinetic energy of the convective motion. In a steady state, the radial gradient of the magnetic field inside the tube is balanced by the gas-kinetic pressure gradient, and the kinetic energy of the convective flux is spent to sustain the field E_r and the Hall current j_φ.

Region 2 is located in the lower photosphere or immediately under it. In this region, the electric current I flowing through the magnetic loop is closed. The electric current distribution in the photosphere, found from magnetic field measurements [21], indicates the presence of noncompensated electric currents [17], i.e., the electric current in the magnetic tube flows through the coronal part of the loop from one footpoint to another. No signatures of the back current have been found. The current is closed in the subphotospheric region (the level $\tau_{5000} = 1$), where the plasma conductivity is isotropic and the current flows along the shortest route from one loop's footpoint to another. Calculations [20] show that at $V_r = 0.1$ km s^{-1} the radius of the tube formed at a height of 500 km above the level $\tau_{5000} = 1$ is $r \approx 3.3 \times 10^7$ cm, and the current is $I \approx 3 \times 10^{11}$ A for the magnetic field $B = 1000$ G at the loop axis.

Region 3 is the coronal part of the loop. Here, the gas-kinetic pressure is below that of the magnetic field (the plasma parameter $\beta \ll 1$) and the loop structure is force-free, i.e., the electric field lines are parallel to the magnetic field lines.

The generalized Ohm law

$$\mathbf{E}^* = \frac{\mathbf{j}}{\sigma_0} + \frac{\mathbf{j} \times \mathbf{B}}{enc} - \frac{\nabla p_e}{en} + \frac{F}{cnm_i\nu_{ia}} \left[(n_a m_a \mathbf{g} - \nabla p_a) \times \mathbf{B} \right] - \frac{F^2}{cnm_i\nu_{ia}}\, \rho\, \frac{\mathrm{d}\mathbf{V}}{\mathrm{d}t} \times \mathbf{B}\,, \tag{1}$$

along with the Maxwell equations, the equation of plasma motion as a whole:

$$\rho\, \frac{\mathrm{d}\mathbf{V}}{\mathrm{d}t} = \rho \mathbf{g} - \nabla p + \frac{1}{c}\, \mathbf{j} \times \mathbf{B}\,, \tag{2}$$

and the continuity equation

$$\frac{\partial \rho}{\partial t} + \operatorname{div}(\rho \mathbf{V}) = 0 \tag{3}$$

self-consistently describes the behavior of the plasma and electromagnetic fields in the flare arch with electric current [13, 18, 20]. Here, F is the relative density of the neutrals, and $\mathbf{E}^* = \mathbf{E} + \mathbf{V} \times \mathbf{B}/c$. The remaining notions are well known.

The Joule dissipation of the current, $q = \mathbf{E}^*\mathbf{j}$, taking into account formulas (1) – (3) is represented in the form [13]

$$q = \frac{j^2}{\sigma_0} + \frac{F^2}{c^2 nm_i\nu_{ia}} (\mathbf{j} \times \mathbf{B})^2\,. \tag{4}$$

It can be seen that in the force-free ($\mathbf{j} \parallel \mathbf{B}$) field the second term is insignificant and the current dissipation is determined by the Spitzer conductivity σ_0. The dissipation is most effective at $\mathbf{j} \perp \mathbf{B}$. The reason for the enhanced current dissipation (the Cowling resistance) in the coronal arch can be the balloon mode of flute instability of the chromosphere or the protuberance above the arch (see Fig. 1). The 'tongue' of partially ionized plasma penetrating into the current channel deforms the magnetic field, thus providing nonstationarity and injection of neutrals into the current channel. As a result, an Ampere force appears that provides enhanced current dissipation. By integrating formula (4) over the arch's volume, we find the power of energy release:

$$\frac{\mathrm{d}W}{\mathrm{d}t} = \left[\frac{m_e(\nu_{ei}+\nu_{ea})d}{e^2 nS} + \frac{2\pi F^2 I^2 d}{c^4 n m_i \nu_{ia} S^2}\right] I^2 = \left[R_c + R_{nl}(I)\right] I^2\,, \tag{5}$$

where S is the cross section of the arch, and d is the size of the flute 'tongue'. The effect of significant Joule dissipation increase in partially ionized gas was first noted by Schluter and Biermann [22]. This effect is due to large energy loss by ions moving through a gas of neutral particles under the action of the Ampere force $\mathbf{j}\times\mathbf{B}$. Estimates [13, 18] suggest that for the current $I \approx 3\times 10^{11}$ A, the Cowling resistance in the chromosphere is $R_{nl} \approx 10^{-2}\ \Omega$, and in the corona $R_{nl} \approx 10^{-3}-10^{-4}\ \Omega$, which provides the observed flare power of about $10^{19}-10^{21}$ W. Note that the 'anomalous' resistance due to the Buneman or ion–sound instabilities can exceed the Cowling resistance only when the current in the arch is filamented with the cross-section area of the current filaments $S_{fil} \approx 10^9-10^{11}\ \mathrm{cm}^2 \ll S \approx 10^{16}-10^{18}\ \mathrm{cm}^2$.

2.2 The flare arch as an equivalent *RLC* circuit

By excluding velocity variations from equations (1) and (2) and expressing electric field through electric current variations and then integrating over the magnetic loop volume, we obtain the equation for low-amplitude current oscillations $|I_\sim| \ll I$ [23]:

$$\frac{1}{c^2}\,L\,\frac{\partial^2 I_\sim}{\partial t^2} + R(I)\,\frac{\partial I_\sim}{\partial t} + \frac{1}{C(I)}\,I_\sim = 0\,. \tag{6}$$

Here, the following notation was used:

$$R \approx 4\,\frac{I^2 l F^2}{c^4 n m_i \nu_{ia} \pi r^4}\,, \quad C \approx \frac{c^4 n m_i S^2}{2\pi l I^2}\,, \quad L \approx 4l\left(\ln\frac{8l}{\pi r} - \frac{7}{4}\right), \tag{7}$$

where l is the major radius of a loop. From relationships (7) it follows that the flare arch has the proper oscillation period which for a sufficiently large current is inversely proportional to its value [23]:

$$P = \frac{2\pi}{c}\,\sqrt{LC(I)} \approx 10\,\frac{S_{17}}{I_{11}}\ [\mathrm{s}]\,, \tag{8}$$

where $S_{17} = S/10^{17}$ [cm^2], and $I_{11} = I/10^{11}$ [A]. These oscillations are distinguished by a high quality factor

$$Q_{RLC} = \frac{1}{cR}\sqrt{\frac{C}{L}} \sim 10^2-10^4\,. \tag{9}$$

The proper *RLC*-oscillations of the magnetic arch modulate its radiation intensity of both a thermal and nonthermal nature. Using formula (8), one can determine the electric current amplitudes from pulsation periods of solar flare radiation. Table 1 lists the date and time (UT) of millimeter wave bursts with pulsations, which were observed over a period 1989–1993 by the Metsähovi solar radio telescope (Finland), and their characteristics for typical sizes of flare arches in the Sun [23]. A spectral analysis revealed the radiation modulation with periods from 0.7 to 17 s, which gives the electric current $I \approx 6\times 10^{10}-1.4\times 10^{12}$ A. The total energy of the electric current, stored in the circuit, amounts to $LI^2/2 \approx 10^{30}-5\times 10^{32}$ erg.

Table 1. Characteristics of millimeter wave solar radiation bursts with high-quality pulsations (Metsähovi) and parameters of the equivalent *RLC* circuit.

Date	Time of the burst (UT)	Flux, s.f.u.*	P, s	I, 10^{11} A	$LI^2/2$, 10^{31} erg	Flare energy, 10^{29} erg
22.06.89	14:47–14:59	< 150	5.2	2.0	1.0	1.0–4.5
19.05.90	13:15–13:40	10	0.7	14.2	50.0	—
01.09.90	7:06–7:30	27	1.1	9.1	20.9	—
24.03.91	14:11–14:17	< 700	10.0	1.0	0.25	—
07.05.91	10:36–11:00	18	8.3	1.2	0.36	1.3–1.8
16.02.92	12:36–13:20	≈ 2000	5.0	2.0	1.0	—
08.07.92	9:48–10:10	≈ 2500	3.3	3.0	2.3	—
08.07.92	10:15–11:00	15	16.7	0.6	0.08	—
27.06.93	11:22–12:00	40	3.5	2.8	2.0	—

* s.f.u. – solar flux unit.

The stored energy was compared with the flare energy for two events (22.06.89 and 07.05.91). In these flares, $\leqslant 5\%$ of the energy stored in the flare arch was released. Such a situation is realized when the magnetic structure is not destroyed after the flare.

As the solar flare is accompanied by current dissipation, the frequency of *RLC*-oscillations must decrease during the flare. In contrast, if the current builds up in the arch as a result of the photospheric emf action, the frequency of *RLC*-oscillations will increase. The search for signals with linear frequency modulation (LFM) (whose frequency is $\omega = \omega_0 + Kt$, where K is a constant) with positive and negative frequency drifts in the low-frequency (LF) modulation spectrum of flare emission, observed at a frequency of 37 GHz by the Metsähovi radio telescope, was carried out in Ref. [24] using the Wigner–Ville transform [25]. An example of such an analysis is shown in Fig. 2.

In the event on 24.03.91, the current in the loop decreased from 9×10^{11} A at the beginning of the burst to 10^{11} A at the final stage. The power released was 10^{21} W. After the flare (14:50 UT), the drift velocity of the LFM signal became positive, indicating that the energy accumulation starts again. This example can be considered as experimental evidence for

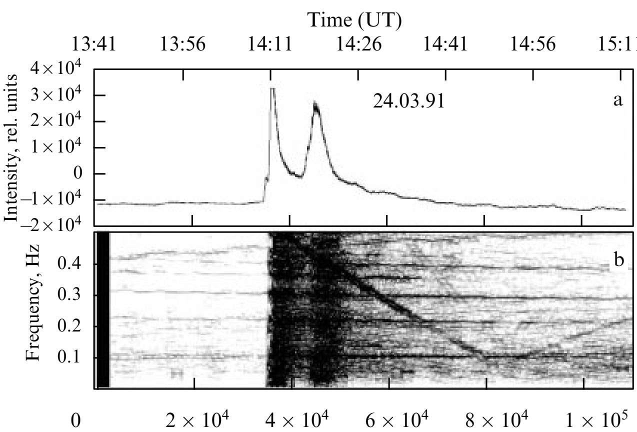

Figure 2. Burst of solar flare emission on 24.03.1991 (14:05 UT) from active region S25W03 at a frequency of 37 GHz and the dynamical spectrum of its pulsations [24].

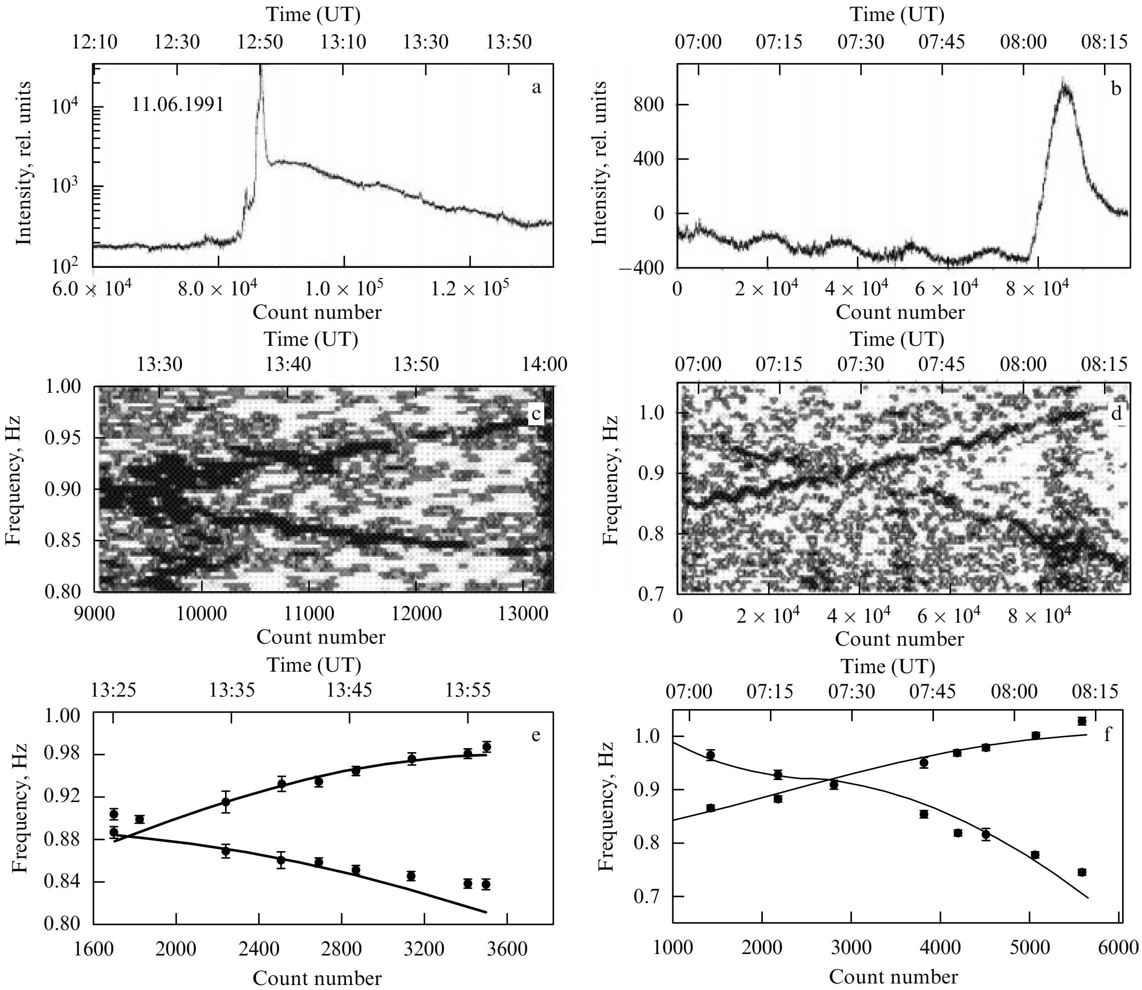

Figure 3. Emission time profiles of solar flares dated 11.05.1991 (a) and 13.07.1992 (b) at the frequency 37 GHz (Metsähovi); (c, d) dynamical spectra of the LF-modulation of the emission as obtained by the Wigner – Ville method; (e, f) results of modeling these dynamical spectra by *RLC*-oscillations of two inductively interacting magnetic arches [26].

the dissipation and storage of energy of electric current in coronal arches.

2.3 Inductive interaction of two current-carrying arches

Equation (6) is valid for a loop magnetically isolated from surrounding loops, i.e., it ignores the mutual induction effect due to the external magnetic flux changing through the loop contour. This effect can be included into integration of the generalized Ohm law by adding to the quantity

$$\int \frac{\partial E_z}{\partial t}\, \mathrm{d}l = -\frac{L}{c^2}\frac{\partial^2 I}{\partial t^2}$$

the electromotive force of the mutual induction, viz.

$$\frac{1}{c^2}\frac{\partial^2}{\partial t^2}\left[\sum_j^N M_j I_j\right],$$

where I_j is the current in the jth loop, M_j is the mutual induction coefficient between the jth loop and the considered one, and the summation is performed over loops surrounding the preferred one. The influence of the surrounding loops can be ignored when studying relatively rapid *RLC*-oscillations of the electric current in the loop. Slow current variations due to induction interaction with surrounding loops will lead to the *RLC*-frequency drift, which must be manifested in the LF spectra. The reason for slow current variations can be the induction emf that appears during interaction of a magnetic loop with other loops in the course of their rising or relative motion. Equations for slow current variations in two induction-interacting magnetic loops are written down in the following form [26] :

$$\begin{aligned} &\frac{1}{c^2}\frac{\partial}{\partial t}(L_1 I_1 + M_{12} I_2) + I_1 R_1(I_1) = \Xi_1\,, \\ &\frac{1}{c^2}\frac{\partial}{\partial t}(L_2 I_2 + M_{21} I_1) + I_2 R_2(I_2) = \Xi_2\,. \end{aligned} \tag{10}$$

Here, $L_{1,2}$ and $R_{1,2}(I_{1,2})$ are the inductances and resistances of the loops, respectively, defined by formulas (7), and $\Xi_{1,2}$ are electromotive forces in the photospheric footpoints of the loops. The mutual induction coefficients can be approximated by the formula

$$M_{12} = M_{21} = 8(L_1 L_2)^{1/2}\,\frac{R^{(1)}_{\mathrm{loop}} R^{(2)}_{\mathrm{loop}}}{(R^{(1)}_{\mathrm{loop}} + R^{(2)}_{\mathrm{loop}})^2 + d^2_{1,2}}\cos\varphi\,, \tag{11}$$

where $R^{(1,2)}_{\mathrm{loop}}$ are the major radii of the loops, $d_{1,2}$ are the distances between the centers of the toroids, and φ is the angle

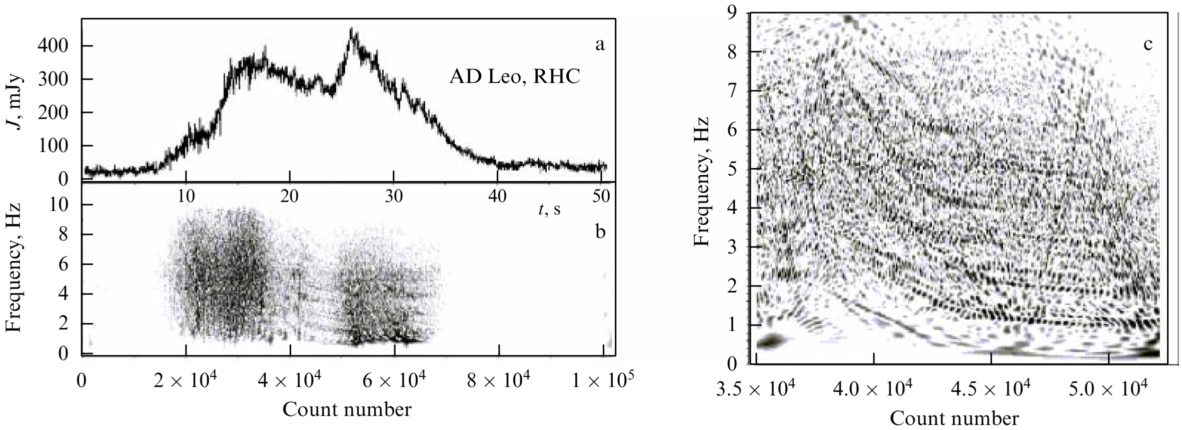

Figure 4. (a) Light curve of a flare from AD Leo on May 19, 1997 at the frequency 4.85 GHz, obtained on the right-hand circular (RHC) polarization of waves. J is the radiation flux (the maximum value reaches 400 mJy), and the flare duration is 50 s. (b) The spectrum of pulsations obtained by the Wigner – Ville method. (c) A zoomed fragment of the spectrum [27].

between normals to the toroid planes. Equations (10), (11) were used in Ref. [26] to model binary tracks that appear in the low-frequency modulation spectra of the flare microwave radiation intensity (Fig. 3).

2.4 Pulsating radio bursts from AD Leo star

Solar – stellar analogs are successfully applied to explain stellar activity. This can be exemplified by an analysis of radio emission from the active red dwarf AD Leo. Observations revealed quasiperiodic pulsations with periods from 1 to 10 s. Phenomenologically, the stellar pulsations are similar to pulsations of type IV solar radio emission, but there are also some differences.

A dynamical spectrum of radio pulsations from an AD Leo flare registered on May 19, 1997 (18.57 UT) by the Effelsberg 100-m radio telescope was calculated in Ref. [27] (Fig. 4). The time profile (Fig. 4a) illustrates fluctuations of radio radiant flux, which have a pulsational character in the dynamical spectrum of the burst (Fig. 4b).

Figure 4c depicts a fragment of the pulsation spectrum in the 0 – 9-Hz range, obtained by the Wigner – Ville transform for the decaying part of the first emission pulse. The spectrum suggests two independent types of modulation simultaneously acting on the radio source: (1) periodic short pulses with the pulse repetition rate $\nu_1 = 2$ Hz, and (2) a sine wave with the frequency $\nu_2 = 0.5$ Hz. A preliminary analysis of pulsations from AD Leo [28] demonstrated that the source of the radio flare on May 19, 1997 was a coronal magnetic arch with the particle number density $n \approx 2.3 \times 10^{11}$ cm^{-3}, temperature $T = 3 \times 10^7$ K, and magnetic induction $B = 730 - 810$ G. Based on these data, it can be concluded that the pulse modulation is due to fast magnetoacoustic oscillations of the magnetic loop with the frequency $\nu_1 \approx V_A/r$, where $V_A = B/\sqrt{4\pi m_i n}$ is the Alfvén velocity, and r is loop's radius. Assuming $\nu_1 = 2$ Hz, the Alfvén velocity is estimated to be $V_A \approx 3.5 \times 10^8$ cm s^{-1}, and $r \approx 1.8 \times 10^8$ cm, which is comparable to the radius of flare magnetic arches in the Sun.

The sinelike modulation (see Fig. 4) is most likely attributed to oscillations of the magnetic arch as an equivalent *RLC* circuit with period (8). The negative frequency drift of the modulating signal is explained by the dissipation of the electric current during the flare. Using $\nu_2 = 0.5$ Hz and peculiarities of the LFM-signal spectrum, we can evaluate the flare arch length of AD Leo to be $l \approx 4 \times 10^{10}$ cm, which is on the order of the radius of the star, the value of the electric current $I \approx 4.5 \times 10^{12}$ A, the energy $W \approx LI^2/2 \approx 5.5 \times 10^{26}$ J of the electric current stored in the flare, and the energy release rate $\dot{W} \approx 10^{25}$ W [27]. The last quantity is 3 – 4 orders of magnitude higher than that in a solar flare. This is due to large magnetic fields on the red dwarf surface and an enhanced photospheric convection.

3. Acceleration of charged particles and their propagation features

3.1 Charged particle acceleration in the flare

A substantial fraction of flare energy is released in the form of energetic particles. In this case, electrons and ions are accelerated up to energies 100 keV and 100 MeV, respectively [29], thus producing hard X-ray and gamma radiation. According to a nonthermal model, an impulsive solar flare produces 10^{37} electrons per second with energies above 20 keVfor 100 s. This means that the energy release rate in the form of accelerated electrons equals 3×10^{29} erg s^{-1}, which corresponds to a total electron energy $E_e\,(>20\text{ keV}) \approx 3 \times 10^{31}$ erg for a total number of accelerated electrons equal to $N_e\,(>20\text{ keV}) \approx 10^{39}$. Requirements for the acceleration rate are less stringent in the hybrid model [30] which assumes an X-ray emission spectrum below 30 keV as originating from the radiation of hot ($T \sim 3 \times 10^7$ K) plasma; at higher energies, radiation is generated by fast electrons. In that case, the required production rate of electrons with energies above 20 keV reduces to 2×10^{35} electrons per second. For an acceleration process duration of 100 s this yields $N_e\,(>20\text{ keV}) \approx 2 \times 10^{37}$ and $E_e\,(>20\text{ keV}) \approx 6 \times 10^{29}$ erg. Therefore, to provide the observed flux of fast electrons, a sufficiently large number of particles ($\geqslant 2 \times 10^{37}$) must be being accelerated. What is the particle reservoir if the acceleration occurs in a flare arch? The number of particles in the arch having plasma density 10^{10} cm^{-3}, cross-section area 10^{18} cm^2, and length $(1-5) \times 10^9$ cm ranges $(1-5) \times 10^{37}$. Any conceivable mechanism accelerates only an insignificant fraction of particles, so that the number of accelerated electrons in the coronal arch proves to be insufficient for providing acceleration even in the favorable case of the hybrid model ($\sim 2\times10^{37}$ electrons). In this connection, *the problem of involving a sufficient number of charged particles into the acceleration process emerges*.

In a magnetic arch, two potential sources can supply the required number of particles. The first source is related to the chromospheric part of the arch, where there are $\sim 5\times10^{40}$ particles in the column with a length extending from the minimum temperature layer to the transition region, if one assumes the loop's cross-section area to be of about 10^{18} cm^2. The second possibility of enriching the flare loop with charged particles emerges during its interaction with dense matter of the prominence, which yields $\approx 3\times10^{38}$ particles [13]. This implies that in order to supply the acceleration mechanism with particles during energetic flares, the chromospheric part of the coronal arch should be the preferential location for the acceleration region. For moderate flares, the acceleration region can lie near the top of the arch.

To explain the generation of fast particles in flares, different acceleration mechanisms have been invoked: stochastic acceleration by waves, acceleration by shocks, betatron acceleration, and acceleration in quasistationary (DC) electric fields. The most effective acceleration is provided by the large-scale electric field $\mathbf{E}$ of the flare magnetic loop. If a magnetic field $|\mathbf{B}| > |\mathbf{E}|$ is present in the plasma, particles will be accelerated only by the projection of the electric field onto the magnetic one, $E_\parallel = \mathbf{EB}/B$. If the value of $E_\parallel$ is below the Dreicer field $E_{\mathrm{D}} = e\Lambda\omega_{\mathrm{p}}^2/V_T^2$, then electrons with the velocities $V > (E_{\mathrm{D}}/E_\parallel)^{1/2} V_T$ (where V_T is the thermal electron velocity, Λ is the Coulomb logarithm, and ω_{p} is the Langmuir frequency) start accelerating (and are known as runaway electrons). The production rate of runaway electrons is given by [31]

$$\dot{N}_{\mathrm{e}} = 0.35\, n\nu_{\mathrm{ei}} V_{\mathrm{a}} x^{3/8} \exp\left(-\sqrt{2x} - \frac{x}{4}\right), \qquad (12)$$

where $x = E_{\mathrm{D}}/E_\parallel$, and V_{a} is the acceleration region volume. The strongest electric fields are generated at the magnetic loop footpoints where an effective charge separation emerges due to the convective flux of the photospheric matter into the tube and a different degree of magnetization of electrons and ions. The expression for $E_\parallel$ was derived in Ref. [32]:

$$E_\parallel \approx \frac{1-F}{2-F}\,\frac{\sigma_0 V_r B^2}{enc^2(1+\mu B^2)}\,\frac{B_r}{B}\,. \qquad (13)$$

Here, the radial component of the magnetic field is $B_r \ll B$, and $\mu = \sigma_0 F^2/(2-F)c^2 n m_{\mathrm{i}} \nu_{\mathrm{ia}}$. The particle acceleration due to the charge-separating field can occur when flute instability is set in at the loop footpoints, when the plasma 'tongue' invading the current channel is inhomogeneous in height. The accelerating field at $B_r \approx 0.1B$ can attain the value of the Dreicer field and even exceed it [32]. All electrons then undergo runaway, and the electric field becomes as high as 17 V cm^{-1}. This makes it possible for particles to acquire a maximum possible energy of ~ 1 GeV on the scale of length of about 10^8 cm. The extremal electric fields are set in for magnetic fields $\sim 10^3$ G and under strong heating of the photospheric footpoints of the magnetic arch, which does not occur in all flares. However, this demonstrates possibilities of the current-carrying magnetic arches to efficiently accelerate particles. For acceleration at the chromospheric footpoints of the arch, the production rate of energetic electrons will exceed 10^{35} electrons per second, which is sufficient for the hybrid model on the assumption of $n = 10^{11}$ cm^{-3} inside the acceleration region, the tube radius 10^8 cm, $T = 10^5$ K, and the acceleration region height $h = 10^8$ cm. Then, $x = E_{\mathrm{D}}/E_\parallel = 26$, $E_\parallel \approx 2\times10^{-3}$ V cm^{-1}, and the energy of the greater part of accelerated electrons will reach 200 keV.

A good illustration of the charged particle acceleration in quasistationary electric fields, when electrons and ions are accelerated in opposite directions, is provided by the flare of July 23, 2002. According to the RHESSI data [33], the X-ray emission in the range from 150 to 200 keV, generated by fast electrons, emanates from one footpoint of the flare arch, while gamma-ray emission line 2.223 MeV generated by fast ions originates from another one.

As the acceleration mechanism produces $\geqslant 10^{35}$ electrons per second, the electric current $I \geqslant 10^{15}$ A is set in. By flowing along the magnetic arch with cross-section area $\sim 10^{18}$ cm^2, this current must induce a magnetic field $B \geqslant 6\times10^6$ G, which is not observed in coronal arches (*the Colgate paradox*). Two possibilities of resolving this paradox have been discussed. The first possibility assumes that the current channel can be split into many current filaments with currents flowing in opposite directions in the neighboring filaments, which results in a total magnetic field below the observed value [34]. It is unclear, however, how filaments with opposite directions of currents can emerge in the accelerated electron beam. Another possibility is related to the formation of reverse current in plasma [35]. Let an electron beam be injected into a plasma along the external magnetic field B_z. Then the field B_φ at any given point in the plasma will change with time as the leading edge of the flux propagates. Changing B_φ gives rise to an electric field E_z appearing at the leading edge of the propagating electron beam. This field acts on plasma electrons in such a way that a current opposite to the injected one appears. Hence, the total current is reduced until complete compensation. According to the Lentz rule, the beam of accelerated electrons can propagate in plasma without expending energy to modify the magnetic field.

3.2 Turbulent regime of propagation of energetic particles

The wave – particle interaction in the solar corona manifests itself in the peculiar character of propagation of energetic particles. For example, in the flare of August 28, 1999 [36], relativistic electrons generating synchrotron radiation at the frequency 17 GHz moved along a coronal magnetic arch with a velocity 30 times less than the speed of light (Fig. 5). This phenomenon can be explained in terms of strong turbulent diffusion [37, 38]. A low-frequency whistler turbulence excited by the electron flux effectively scatters relativistic particles through the pitch angle. As a result, instead of freely propagating, the electrons, due to the anomalous (turbulent) viscosity, move with a velocity on the order of the phase velocity of whistlers, namely $\approx 0.03c$ (line A). At the next injection (line B), whistles did not affect the particle propagation.

The absence of noticeable ($< 0.07\%$) linear polarization of the H_α-emission generated by energetic proton beams decelerating in the chromosphere [30] provides the second example. The most likely reason for this occurring is the scattering of the radiation on small-scale Alfvén waves excited at the ion cyclotron resonance by protons with energies ~ 1 MeV, which leads to radiation isotropy. Here, protons are effectively scattered through pitch angles (strong diffusion) if the power of the energy particle accelerator

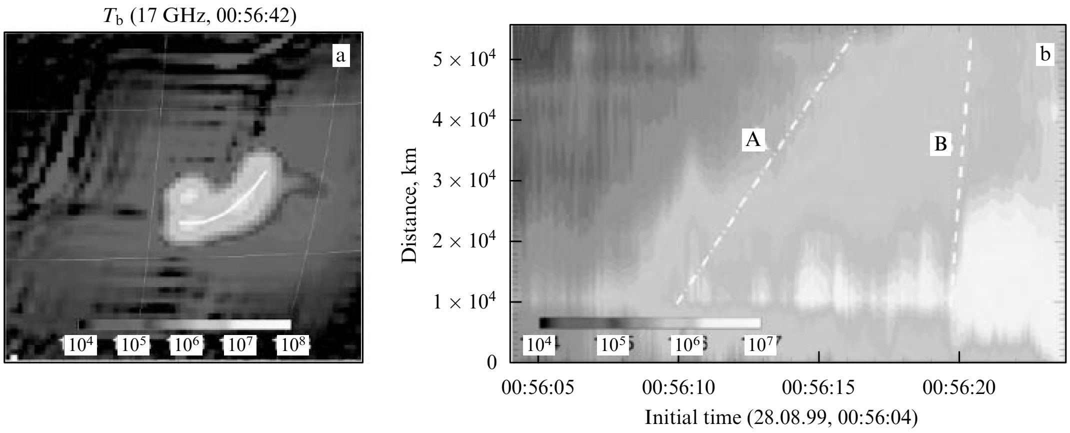

Figure 5. (a) The image of the flare dated 28.08.1999, consisting of two sources and obtained by the Nobeyama radioheliograph at the frequency 17 GHz at 00:56:42 UT. The light line in the center of the figure shows the trajectory of relativistic electrons propagating in an extended arch 5×10^4 km in length [36]. T_b is the brightness temperature of the microwave radiation, $10^4 < T_b < 10^8$ K. The lighter regions correspond to higher temperatures. (b) The propagation of the microwave signal with the velocity $v = 0.03c$ at the first stage of acceleration of energetic electrons (line A), and with the velocity $v \sim c$ at the second acceleration stage (line B).

exceeds $J_* = 5 \times 10^{12}$ protons per cm^2 per s. The data on energetic particles in solar flares suggest an acceleration rate of protons with energies above 1 MeV on the order of $10^{33}-10^{34}$ protons per s [29]. Assuming the area of the proton invasion region into the chromosphere to be $\sim 10^{18}$ cm^2, we find the flux $J \sim (10^{15}-10^{16})$ cm^{-2} s^{-1} $\gg J_*$. The strong diffusion regime also leads to a time delay of the gamma-ray line emission relative to hard X-ray emission from flares [40], since the velocity of the turbulent front created by ions is an order of magnitude below that of the turbulent 'wall' formed by fast electrons.

4. Eigen-mode oscillations of loops and flare plasma diagnostics

The TRACE satellite observations of the Sun discovered oscillations of the coronal arches above active regions [41], which stimulated the development of a promising field in astrophysics — coronal seismology. These studies were initiated by Dutch physicist H Rosenberg [42] who related pulsations of type IV solar radio emission to magnetohydrodynamic (MHD) oscillations of the coronal arch. At the boundary between the arch and the external medium there is an impedance jump for MHD waves, so that the coronal arch can be considered a resonator. Pulsating emission over different wavebands (optical, X-ray, radio) is observed not only from the Sun, but also from flare stars. Interest in oscillations of arches is related to feasibility of explaining coronal heating mechanisms and upgrading flare diagnostic techniques.

Coronal arch oscillations are studied by modeling a plasma cylinder with radius r and length l with ends 'frozen' into a superconducting medium. Plasma parameters inside and outside the cylinder are the following: density ρ_i, temperature T_i, and magnetic field B_i, as well as ρ_e, T_e, and B_e, respectively. The dispersion equation relating the cylinder oscillation frequency ω to the wave vector components $k_\perp$ and $k_\parallel$ has the form [43, 44]

$$\frac{J'_m(\varkappa_i r)}{J_m(\varkappa_i r)} = \alpha \, \frac{H_m^{(1)'}(\varkappa_e r)}{H_m^{(1)}(\varkappa_e r)} \,, \tag{14}$$

where

$$\varkappa^2 = \frac{\omega^4}{\omega^2(C_S^2 + V_A^2) - k_\parallel^2 C_S^2 V_A^2} - k_\parallel^2 \,,$$

$$\alpha = \frac{\varkappa_i \rho_i}{\varkappa_e \rho_e} \, \frac{\omega^2 - k_\parallel^2 V_{Ai}^2}{\omega^2 - k_\parallel^2 V_{Ae}} \,,$$

C_S is the speed of sound, J_m and $H_m^{(1)}$ are the Bessel and Hankel functions of the first kind, respectively, $k_\parallel = \pi s / l$, and $s = 1, 2, 3, \ldots$. For a thin $(r/l \ll 1)$ and dense $(\rho_e/\rho_i \ll 1)$ cylinder at $m = 0$, from formula (14) it follows that the frequency of fast magnetosonic (sausage) oscillations, which mostly modulate emission from arches, is given by

$$\omega_+ = (k_\perp^2 + k_\parallel^2)^{1/2} (C_{Si}^2 + V_{Ai}^2)^{1/2} \,. \tag{15}$$

The transverse wave number is $k_\perp = \lambda_i / r$, where λ_i are zeros of the Bessel function, and $J_0(\lambda) = 0$. Estimates [45] show that the electron plasma heat conductivity is the most important reason for sausage oscillation decay in solar arches. Therefore, their quality factor is defined as

$$Q = \frac{\omega_+}{\gamma} \approx \frac{2 m_e}{m_i} \, \frac{P \nu_{ei}}{\beta^2 \sin^2 2\theta} \,, \tag{16}$$

where $\theta = \arctan(k_\perp / k_\parallel)$, $P = 2\pi/\omega_+$ is the period of oscillations, and γ is the wave decay decrement. In the course of sausage oscillations, modulation of the flux of gyrosynchrotron emission of energetic electrons with a power-law energy spectrum with index δ for an optically thin source has the form [45]

$$\varDelta = 2\xi \, \frac{\delta B}{B} = \xi \beta \,, \qquad \xi = 0.9\delta - 1.22 \,. \tag{17}$$

Taking into account the curvature of magnetic field and a sufficiently large parameter β, the balloon mode of flute instability can be excited in coronal arches. The ballooning oscillations result from the joint action of the destabilizing force $F_1 \sim p / R_{loop}$ related to the pressure gradient and the

Table 2. Formulas to determine parameters of a flare from emission pulsations caused by ballooning and sausage oscillations of a magnetic arch. Here, $\chi = 10\varepsilon/3 + 2$, $\tilde{r} = 2.62r$, $\varepsilon = \Delta/\xi$, temperature T is expressed in K, particle number density n is in cm^{-3}, and magnetic field B is in G.

Ballooning oscillations	Sausage oscillations
$T = 2.42 \times 10^{-8}\,\dfrac{l^2\varepsilon_1}{N^2P_1^2}$	$T = 1.2 \times 10^{-8}\,\dfrac{\tilde{r}^2\varepsilon}{P^2\chi}$
$n = 5.76 \times 10^{-11}\,\dfrac{Q_1 l^3\varepsilon_1^{7/2}}{N^3P_1^4}\sin^2 2\theta$	$n = 2 \times 10^{-11}\,\dfrac{Q\tilde{r}^3\varepsilon^{7/2}}{P^4\chi^{3/2}}\sin^2 2\theta$
$B = 6.79\times10^{-17}\,\dfrac{Q_1^{1/2}l^{5/2}\varepsilon_1^{7/4}}{N^{5/2}P_1^3}\sin 2\theta$	$B = 2.9\times10^{-17}\,\dfrac{Q^{1/2}\,\tilde{r}^{5/2}\varepsilon^{7/4}}{P^3\chi^{5/4}}\sin 2\theta$

curvature of magnetic field and the restoring force $F_2 \sim B^2/R_{\text{loop}}$ arising from the tension of the magnetic field lines. The period of oscillations equals

$$P_1 = \frac{2l}{V_{\text{A}}}\left(N^2 - \frac{l\beta}{2\pi d}\right)^{-1/2} \approx \frac{2l}{V_{\text{A}}N}\,, \tag{18}$$

where N is the number of oscillating regions present along the loop's length l. Estimates indicate that the ballooning oscillations in the atmosphere of the Sun also decay because of electron plasma heat conductivity. Equations for the frequency of oscillations (15), (18), the quality factor (16), and the emission modulation depth (17) can be used for determining the temperature and density of plasma and the magnetic field in the arch (Table 2).

Two examples of applying such diagnostic techniques are given in Ref. [45]. Observations of the solar flare of May 8, 1998 (01:49 – 02:17 UT) in the form of a single arch at the frequency 17 GHz (the Nobeyama radioheliograph) and in the hard X-ray range (the Yohkoh satellite) testify to the presence of ballooning oscillations with the parameters $l = 8 \times 10^9$ cm, $N = 4$, $\theta = 66°$, $\Delta_1 \approx 0.3$, $Q_1 \approx 25$, and $\delta = 3.5$. Using formulas from Table 2, we find $T \approx 5.9 \times 10^7$ K, $n \approx 1.4 \times 10^{11}$ cm^{-3}, $B \approx 425$ G, and the plasma parameter $\beta \approx 0.16$.

The solar flare of August 28, 1999 (00:55 – 00:58 UT) illustrates the interaction of two arches: a compact one and an extended one (see Fig. 5). A wavelet analysis revealed the characteristic pulsation periods 14 and 2.4 s. The scenario of the event is as follows. The flaring energy release was accompanied by exciting ballooning oscillations with $P_1 = 14$ s in a compact source. The gas pressure increase led to the development of an aperiodic mode of ballooning instability and the interaction of the compact source with the neighboring arch (loop – loop interaction), which was accompanied by an injection of hot plasma and energetic particles. Because oscillations with the period $P = 2.4$ s were set up after the plasma injection, they are most likely due to sausage modes of the extended source. Applying the formulas from Table 2, the analysis of the pulsations yields the following parameters of the compact and extended arches:

$$T \approx 4.6 \times 10^7 \text{ K}, \quad n \approx 10^{11} \text{ cm}^{-3}, \quad B \approx 300 \text{ G}, \quad \beta \approx 0.18\,;$$
$$T \approx 2.1 \times 10^7 \text{ K}, \quad n \approx 10^{10} \text{ cm}^{-3}, \quad B \approx 120 \text{ G}, \quad \beta \approx 0.06\,,$$

respectively. The compact arch is linked to the primary source of energy release and demonstrates higher values of temperature, density and the magnetic field.

5. Conclusion

We have shown that coronal magnetic loops (arches) play an important role in the origin of solar flare activity. Strong electric currents that initiate an explosive energy release, when flute instability develops, can flow in the arches. Flute instability (the ballooning mode) can be responsible both for charged particle acceleration and plasma injection into the neighboring arch via loop – loop interaction.

The mechanism of acceleration in quasistationary electric fields is crucial for particle acceleration in flares. The wave – particle interaction effect determines the dynamics of energetic particles in the solar atmosphere.

The approximation of a current-carrying arch in the form of an equivalent electric circuit and resonator for MHD waves reflects the physics of processes in flares. The flare arch possesses a set of proper frequencies that result in a low-frequency modulation of the emission in a wide wavelength range (optical, radio, X-ray). The rapidly evolving field of modern astrophysics — coronal seismology — based on these approaches provides a powerful diagnostic technique for flare plasma.

This work is supported by the Program 'Solar Activity' of the Presidium of RAS, by the Program OFN-16, and by the RFBR grants 06-02-16859, 04-02-39029GFEN, and 05-02-16252.

References

1. Sweet P A, in *Electromagnetic Phenomena in Cosmical Plasma* (Intern. Astron. Union Symp., No. 6, Ed. B Lehnert) (Cambridge: Univ. Press, 1958) p. 123
2. Gold T, Hoyle F *Mon. Not. R. Astron. Soc.* **120** 89 (1960)
3. Sturrock P A *Astron. J.* (Suppl.) **73** 78 (1968)
4. Heyvaerts J, Priest E R, Rust D M *Astrophys. J.* **216** 123 (1977)
5. Parker E N *Astrophys. J.* **180** 247 (1973)
6. Spicer D S *Solar Phys.* **53** 305 (1977)
7. Sakai J-I, de Jager C *Space Sci. Rev.* **77** 1 (1996)
8. Syrovatskii S I *Astron. Zh.* **43** 340 (1966) [*Sov. Astron.* **10** 270 (1966)]
9. Somov B V *Physical Processes in Solar Flares* (Dordrecht: Kluwer Acad. Publ., 1992)
10. Alfvén H, Carlqvist P *Solar Phys.* **1** 220 (1967)
11. van Hoven G, in *Solar Flare Magnetohydrodynamics* (Fluid Mechanics of Astrophys. and Geophys., Vol. 1, Ed. E R Priest) (New York: Gordon and Breach Sci. Publ., 1984) Ch. 4
12. Melrose D B, McClymont A N *Solar Phys.* **113** 241 (1987)
13. Zaitsev V V, Stepanov A V *Astron. Zh.* **68** 384 (1991) [*Sov. Astron.* **35** 189 (1991)]; *Solar Phys.* **139** 343 (1992)
14. Sen H K, White M L *Solar Phys.* **23** 146 (1972)
15. Henoux J C, Somov B V *Astron. Astrophys.* **185** 306 (1987)
16. Ionson J A *Astrophys. J.* **254** 318 (1982)
17. Melrose D B *Astrophys. J.* **451** 391 (1995)
18. Zaitsev V V, Urpo S, Stepanov A V *Astron. Astrophys.* **357** 1105 (2000)
19. Klimchuk J A et al. *Publ. Astron. Soc. Jpn.* **44** L181 (1992)
20. Khodachenko M L, Zaitsev V V *Astrophys. Space Sci.* **279** 389 (2002)
21. Leka K D et al. *Astrophys. J.* **411** 370 (1993)
22. Schluter A, Biermann L *Z. Naturforsch. A* **5** 237 (1950)
23. Zaitsev V V et al. *Astron. Zh.* **75** 455 (1998) [*Astron. Rep.* **42** 400 (1998)]
24. Zaitsev V V et al. *Astron. Zh.* **80** 945 (2003) [*Astron. Rep.* **47** 873 (2003)]
25. Cohen L *Proc. IEEE* **77** 941 (1989)
26. Khodachenko M L et al. *Astron. Astrophys.* **433** 691 (2005)
27. Zaitsev V V et al. *Pis'ma Astron. Zh.* **30** 362 (2004) [*Astron. Lett.* **30** 319 (2004)]
28. Stepanov A V et al. *Astron. Astrophys.* **374** 1072 (2001)
29. Miller J A et al. *J. Geophys. Res.* (*Space Phys.*) **102** (A7) 14631 (1997)
30. Holman G D, Benka S G *Astrophys. J.* **400** L79 (1992)

31. Knoepfel H, Spong D A *Nucl. Fusion* **19** 785 (1979)
32. Zaitsev V V, Khodachenko M L *Izv. Vyssh. Uchebn. Zaved. Radiofiz.* **40** 176 (1997)
33. Dennis B R *Lect. Not. Phys.* (2005) (in press)
34. van den Oord G H J *Astron. Astrophys.* **234** 496 (1990)
35. Lee R, Sudan R N *Phys. Fluids* **14** 1213 (1971)
36. Yokoyama T et al. *Astrophys. J.* **576** L87 (2002)
37. Bespalov P A, Trakhtengerts V Yu, in *Voprosy Teorii Plazmy* (Problems in Plasma Theory) Vol. 10 (Ed. M A Leontovich) (Moscow: Atomizdat, 1980) p. 88 [Translated into English: *Reviews of Plasma Physics* Vol. 10 (Ed. M A Leontovich) (New York: Plenum Press, 1986) p. 155]
38. Stepanov A V et al. *Publ. Astron. Soc. Jpn.* (2005) (in press)
39. Bianda M et al. *Astron. Astrophys.* **434** 1183 (2005)
40. Bespalov P A, Zaitsev V V, Stepanov A V *Astrophys. J.* **374** 369 (1991)
41. Aschwanden M J et al. *Astrophys. J.* **520** 880 (1999)
42. Rosenberg H *Astron. Astrophys.* **9** 159 (1970)
43. Zaitsev V V, Stepanov A V, in *Issledovaniya po Geomagnetizmu, Aeronomii, Fizike Solntsa* (Studies in Geomagnetism, Aeronomy and Solar Physics) Issue 37 (Moscow: Nauka, 1975) p. 3
44. Nakariakov V M, Stepanov A V *Lect. Not. Phys.* (2005) (in press)
45. Stepanov A V et al. *Pis'ma Astron. Zh.* **30** 530 (2004) [*Astron. Lett.* **30** 480 (2004)]

PACS numbers: 78.70.Bj, **98.35.–a**, **98.70.–f**
DOI: 10.1070/PU2006v049n03ABEH005969

Annihilation emission from the galactic center: the INTEGRAL observatory results

E M Churazov, R A Sunyaev, S Yu Sazonov, M G Revnivtsev, D A Varshalovich

1. Introduction

The narrow positron annihilation line at the energy 511 keV is the brightest line in the emission spectrum of our Galaxy at energies above 10 keV. A spectral feature at energy ~ 476 keV in the radiation from the galactic center region was discovered more than 30 years ago by detectors with low energy resolution during balloon flights [1]. Soon after, observations carried out with high-resolution Ge detectors reliably identified this feature with the narrow positron annihilation line at 511 keV [2]. Later on, the annihilation emission was detected in several other experiments. Despite repeated observations, no final answer on the nature of the annihilation emission of the Galaxy has been obtained so far. This is primarily due to the existence of several principally different mechanisms for producing positrons, including:

radioactive β^+ decay of unstable isotopes, for example, ^{26}Al or ^{56}Co, produced in supernova and nova explosions;

decay of π^+ mesons arising from the interaction of cosmic rays with matter;

electron – positron pair production in high-energy photon interactions or in strong magnetic fields near compact sources — black holes or radio pulsars, and

production of positrons from dark matter particle annihilation.

Although this list is incomplete, it clearly demonstrates a great diversity of mechanisms discussed — from the commonly accepted (supernova nucleosynthesis) to the most exotic (dark matter annihilation).

Key explanations of the nature of the 511-keV line comprise: (a) determination of the space distribution of the annihilation radiation in the Galaxy and its comparison with that of potential positron sources, and (b) detailed studies of the annihilation radiation spectrum and obtaining restrictions on properties of matter in which the annihilation occurs. These are the problems that should be resolved by the INTEGRAL observatory equipped with a high-resolution Ge spectrometer.

2. Observations and data analysis

The INTEGRAL observatory is a project of the European Space Agency with the participation of Russia and the USA. The observatory was launched into a high-apogee orbit with a period of 3 days by the Proton rocket in October 2002. To investigate the annihilation emission, the SPI device [3] consisting of 19 independent high-purity Ge crystals that provide an energy resolution of about 2 keV at 511 keV was used. A tungsten mask with a thickness of 3 cm was installed at 171 cm from the detector. This mask provides modulation of the radiant flux registered by the detector. The field of view of the telescope is around 30°. In our analysis, we have made use of data obtained in the period from February to November 2003. The total observation time amounted to 3.9×10^6 s [4].

The energy scale in each observation was controlled by the location of bright background lines (^{71}Ge, 198.4 keV; ^{69}Zn, 438.6 keV; ^{69}Ge, 584.5 keV, and ^{69}Ge, 882.5 keV) seen in the spectrum taken by each detector. After such calibration, the typical amplitude of variations with time of the background line locations near 500 keV was less than 0.01 keV. The positron annihilation line is also present in the background spectrum of the SPI telescope. This line is due to positrons produced and annihilated inside detector's body and in the surrounding materials exposed to high-energy charged particles. Because the spectral line produced by the positron annihilation in the telescope material was broadened with respect to telescope intrinsic resolution, the actual energy resolution was determined from interpolation of the observed widths of two lines, 438.6 keV and 584.5 keV, symmetrically located around the 511-keV line. The energy resolution at 511 keV, determined in this way, corresponds to 2.1 keV (full width at half maximum, FWHM) for the entire data set.

Modeling the background spectrum of the telescope has required serious effort. During observations of the Galactic Center region, the background flux at 511 keV is approximately 50 – 100 times above the desired signal, and therefore the background model should predict it with an accuracy much better than 1%. To construct the background model, we have used observed data obtained from different regions of the celestial sphere located at angular distances of more than 30° from the center of the Galaxy. The total exposure of observations used to construct the background model was around 3.7×10^6 s. The model accounts for the background variations related to variations in the charged particle flux and the gradual accumulation of long-lived unstable isotopes inside the detector body.

3. The map of the Galaxy in the 511-keV line

Figure 1 shows the map of the surface brightness of galactic emission in the 511-keV line. In each observation, the detected 508 – 514-keV flux (with the model background